Invited Paper

AFM of Self-Organised Nanoparticle Arrays: Frequency Modulation, Amplitude Modulation, and Force Spectroscopy

Adam Sweetman, Peter Sharp, Andrew Stannard,
Subhashis Gangopadhyay, and Philip J. Moriarty

School of Physics and Astronomy, University of Nottingham, Nottingham NG7 2RD, UK

ABSTRACT

Frequency modulation (FM) and amplitude modulation (AM) atomic force microscopy have been used to image self-organised assemblies of octanethiol-passivated Au nanoparticles adsorbed on SiO_2/Si(111) samples (where the oxide is either 200 nm or $\sim$ 2 nm thick). Imaging at negative frequency shifts - i.e. in the attractive force regime - in FM mode in ultrahigh vacuum we measure nanoparticle heights which are over 50 % larger than those measured using conventional ("repulsive mode") tapping mode imaging in air. A similar difference in nanoparticle height is observed for attractive mode imaging in air. For nanoparticles adsorbed on 200 nm thick oxide layers, force-distance ($F(z)$) spectra (measured in FM mode) comprise both a van der Waals component with the conventional power law ($\frac{1}{z^2}$) dependence and a strong electrostatic force which is best fitted using a logarithmic function of the form $ln(\frac{1}{z})$.

Keywords: Nanoparticles; self-organised; atomic force microscopy; force spectroscopy

1. INTRODUCTION

The complex dewetting dynamics of colloidal solutions of nanoparticles (increasingly called "nanofluids") leads to the formation of a rich variety of self-organised nano- and microstructured patterns on solid surfaces.[1–3] Through nucleation-and-growth and/or spinodal processes,[4–7] a broad array of inhomogeneous - but, in many cases, spatially correlated - structures form. These include, for example, foam-like networks,[6–9] labyrinthine assemblies strikingly similar to those formed in polymer and binary fluid phase separation,[4,5,10] and fingering instabilities reminiscent of those formed in Hele-Sham cells and solidification processes.[11,12]

A fascinating area of research relates to the interdependence of the morphological properties of these self-organised patterns and their physicochemical properties including, in particular, their charge transport behaviour. This is an area which has been explored by a number of groups,[13–16] including our own, and builds on the seminal theoretical work of Middleton and Wingreen[17] in the early nineties. Although progress has been made in understanding the relationship between nanoparticle array topology and charge transport pathways via conventional cryogenic I(V) measurements, there has to date been no direct experimental visualisation of the current paths and charge interface movement predicted by theory.[17–19] Local scanning probe methods such as electric force microscopy and scanning capacitance microscopy have immense potential for the visualisation and, indeed, control (via local gating) of charge transport in nanoparticle assemblies. Before these methods can be applied to the study of electrically contacted self-organised assemblies, however, it is important to consider and elucidate the fundamental physical forces which influence scanning probe imaging of nanoparticles on dielectric surfaces. This is the motivation for the research described in this paper.

We have used both frequency modulation (FM) and amplitude modulation (AM) atomic force microscopy to image cellular networks of colloidal nanoparticles formed via the drying of a colloidal solution (as described by, for example, Rabani *et al.*[5] and Martin *et al.*[7]) on solvent- and plasma-cleaned oxide-terminated silicon samples. The gold nanoparticles used throughout our studies have a mean core diameter of 1.8 nm (see Experimental section) and are passivated with octanethiol ligands which, in the all-trans, "zig-zag" conformation have a length of 1.27 nm.[20,21] The mean diameter of the passivated nanoparticles in solution for each of our samples is

Further author information: Please send correspondence to ppxams@nottingham.ac.uk (Adam Sweetman) or philip.moriarty@nottingham.ac.uk (Philip Moriarty)

Nanostructured Thin Films, edited by Geoffrey B. Smith, Akhlesh Lakhtakia,
Proc. of SPIE Vol. 7041, 704102, (2008) · 0277-786X/08/$18 · doi: 10.1117/12.796403

thus 4.3 nm. We find that nanoparticle height values measured in conventional tapping mode imaging are, however, only 35% of this value (1.5 nm). While Chen *et al.*[22] have recently carried out a systematic and careful analysis of the role of imaging parameters on the measured heights of bare (charge stabilised) Au nanoparticles deposited on mica surfaces, here we study *thiol-passivated* particles. Not only does the thiol passivation layer produce hydrophobic nanoparticle surfaces - which contrast with the rather more hydrophilic character of the SiO_2 substrate - but its energy dissipation properties will be significantly different to those of bare Au particles. Each of these effects will contribute to the overall interaction of the AFM tip with the nanoparticle assembly and will thus potentially influence measured height values.

Another important influence on non-contact/tapping mode AFM height measurements is the presence of uncompensated electrostatic forces. As pointed out by Sadewasser *et al.*[23] amongst others, this is a problematic issue when inhomogeneous samples consisting of a two or more materials with different work functions are imaged. Although in UHV non-contact AFM it is common to apply a bias voltage to null out the contact potential, unless the bias voltage is adjusted locally - as in scanning Kelvin probe microscopy -for an inhomogeneous sample there will be an uncompensated electrostatic force due to the variation of the effective contact potential across the surface. Here we use both frequency shift-vs-voltage and force-vs-distance spectroscopy to explore the role of electrostatic forces in the imaging of Au nanoparticle assemblies.

2. EXPERIMENTAL

Octanethiol (C_8)-passivated Au nanoparticles in hexane were synthesised using the method of Brust *et al.*[?] Small angle X-ray scattering studies of identically prepared samples (at the XMaS beamline of the European Syncorotron Radiation Facility) showed that the mean diameter of the nanoparticle core is 1.8 nm. As noted above, when the octanethiol chain length is taken into consideration this means that the overall mean nanoparticle diameter is 4.3 nm. A small volume ($\sim 10\ \mu$l) of the nanoparticle solution was then placed on either a native oxide-terminated or thermal oxide (200 nm)-terminated Si(111) sample which had been cleaned using ultrasonication in solvents followed by exposure to an oxygen plasma for five minutes. The sample was subsequently spun at 4000 rpm for 30 seconds, leading to rapid removal of the solvent and the formation of a cellular network of particles due to nucleation-dominated and/or spinodally-dominated solvent dewetting.[24]

Two types of AFM instrument were used: an ultrahigh vacuum, variable temperature "beam deflection" STM-AFM (Omicron) and an air-based MFP-3D system from Asylum Research. A number of tip types were used. For the air-based measurements we used Olympus AC240 probes (spring constant: 2 Nm^{-1}; resonant frequency 70 kHz; and nominal radius of curvature 10 nm) whereas the UHV work was carried out either with: (i) NSC-16 tips (resonant frequency: 170 kHz; spring constant: 40 Nm^{-1}; silicon; nominal radius of curvature 10 nm; supplied by MikroMasch); (ii) "super-sharp" silicon tips (resonant frequency 190 kHz; spring constant: 48 Nm^{-1}; nominal radius of curvature < 5 nm; supplied by NanoWorld); or (iii) DP16-W probes (resonant frequency: 170 kHz; spring constant: 40 Nm^{-1}; nominal radius of curvature: 1 nm due to presence of W "spike" at the end of the tip; MikroMasch). Throughout the paper we will specify which particular type of tip was used for each measurement.

For the calibration of the amplitude of cantilever oscillation for the UHV AFM measurements we use a well-established method involving the normalised frequency shift,[25] γ given by:

$$\gamma = \frac{\Delta f}{f_0} k A^{\frac{3}{2}} \tag{1}$$

where Δf is the shift in frequency of the cantilever resonance and f_0 is the natural resonant frequency. γ is a function of both d, the distance between the end of the tip and the surface at the lower turning point of the oscillation, and A, the cantilever amplitude. If we vary A but keep γ constant, d does not change. However, this implies that the mean distance of the tip from the surface, z, must change. With the feedback loop switched on this shift in z can be used to determine the cantilver amplitude.

To extract force vs distance information from the measured Δf vs Δz data we use the deconvolution routine put forward by Sader and Jarvis.[26] Details of this deconvolution routine are available in a number of previous publications (including, for example, refs[27,28]) and we therefore do not include a discussion of this topic here. Ref.[28] provides a helpful definition of the force in terms of the distance of closest approach (d above)).

3. RESULTS AND DISCUSSION

As a number of sample environments, imaging modes, and spectroscopies have been used to probe the nanoparticle assemblies, in the following we consider each set of experiments separately before drawing general conclusions in the final section of the paper.

3.1 Frequency Modulation AFM under UHV Conditions

Fig. 1 shows two non-contact AFM images, taken under UHV conditions, of a submonolayer of Au nanoparticles on a 200 nm thick thermally-grown SiO_2 oxide. As outlined above, the holes in the layer seen in Fig. 1(a) arise from solvent dewetting events[4,5,7] during the drying-mediated self-organisation process. It is important to note that the nanoparticle samples we use have a relatively wide size distribution ($\sim \pm 15\%$) and thus the presence of highly ordered superlattices is not expected. It is possible, however, to find small regions of local order. One of these is highlighted in the contrast-enhanced and low pass-filtered region shown towards the centre of Fig. 1(b). In the context of this paper, however, the vertical (height) information is more relevant than the lateral spacing. The average apparent height of the nanoparticles shown in Figs. 1(a) and 1(b) is 2.4 nm (see representative line profile in Fig. 1(c)). The image was acquired with a bias voltage of 2.3 V (to null out the contact potential - see discussion in following sections), a frequency offset of -190 Hz, and a cantilever oscillation amplitude of 14.6 nm.

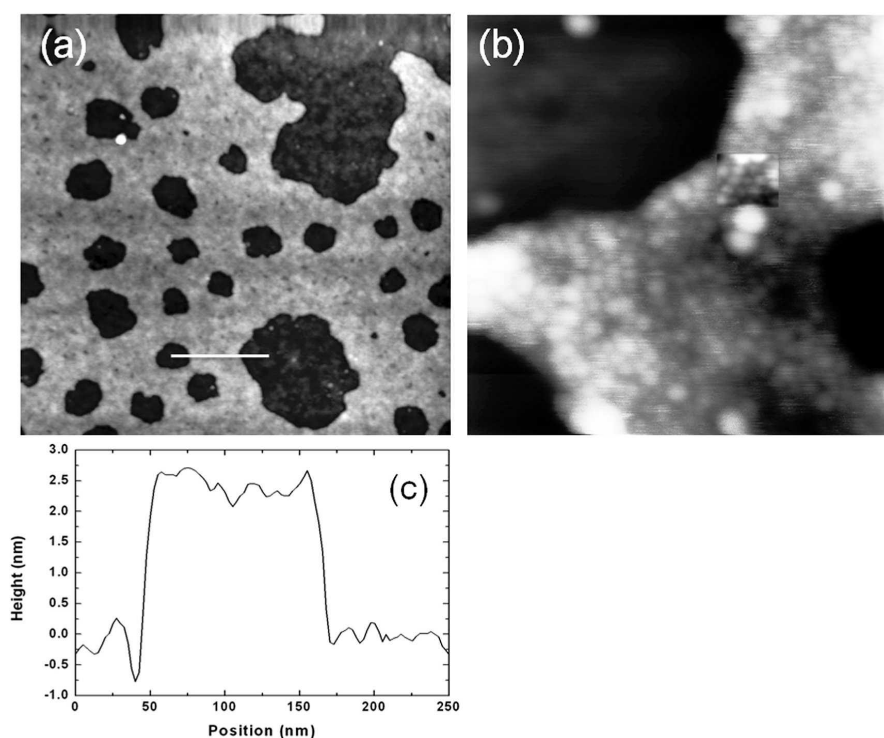

Figure 1. (a) 1 x 1 μm^2 non-contact AFM image of a network of 1.8 nm core diameter octanethiol-passivated Au nanoparticles on a 200 nm thick thermally-grown SiO_2 film on a Si(100) substrate.See text for imaging parameters. (b) 100 x 100 nm^2 image showing small locally-ordered areas of nanoparticles within the network branches. One such region is highlighted in the image via contrast enhancement and a 3 x 3 median smooth. The imaging parameters in this case were V_{gap}=+0.8V, Δf = -150 Hz, and cantilever oscillation amplitude = 14.6 nm. An NSC-16 cantilever (see Experimental section) was used for imaging. (c) Height profile along line shown in (a).

3.2 Attractive vs Repulsive AM AFM: Discrepancies in Nanoparticle Heights

An important question to address is the extent to which the operating environment (UHV vs ambient conditions) affects the imaging process and, thus, the measured height of the nanoparticles. SiO_2 is a hydrophillic substrate

(particularly following plasma cleaning) and will thus readily support a low contact angle water film. Thiol-passivated nanoparticles are, on the other hand, rather hydrophobic. This raises an interesting question regarding the possibility of a switch in the mode of imaging from repulsive to attractive - as suggested by Chen *et al.*[22] for bare Au particles (under appropriate imaging conditions) - as the tip moves from SiO_2 to a nanoparticle-covered region. We therefore imaged a nanoparticle network (formed from the same colloidal solution used to produce the sample shown in Fig. 1) in air using parameters appropriate for imaging in tapping mode (i.e. repulsive mode imaging) and in the non-contact ("attractive") regime. These images are shown in Fig. 2. Analysis of the grey scale distribution of the images (see lower part of Fig. 2) provides a useful tool to determine the average height of the nanoparticles for both regimes of imaging. There is a significant (100 %) difference between the heights of the particles measured in the two imaging regimes. Moreover, the apparent height of the nanoparticles measured in attractive mode in air is similar (but certainly not identical) to the value determined via UHV non-contact imaging (i.e. 2.4 nm). It is likely that the apparent height varies with both the oscillation amplitude and the amplitude setpoint for both modes of imaging (as found by Chen *et al.*[22] for bare Au particles). We are currently carrying out a systematic set of measurements to ascertain the full extent of the variability of height measurements for passivated nanoparticles. Nevertheless, from the present results alone it is clear that a very careful choice of imaging parameters is required for accurate measurement of the diameter of adsorbed passivated Au nanoparticles.

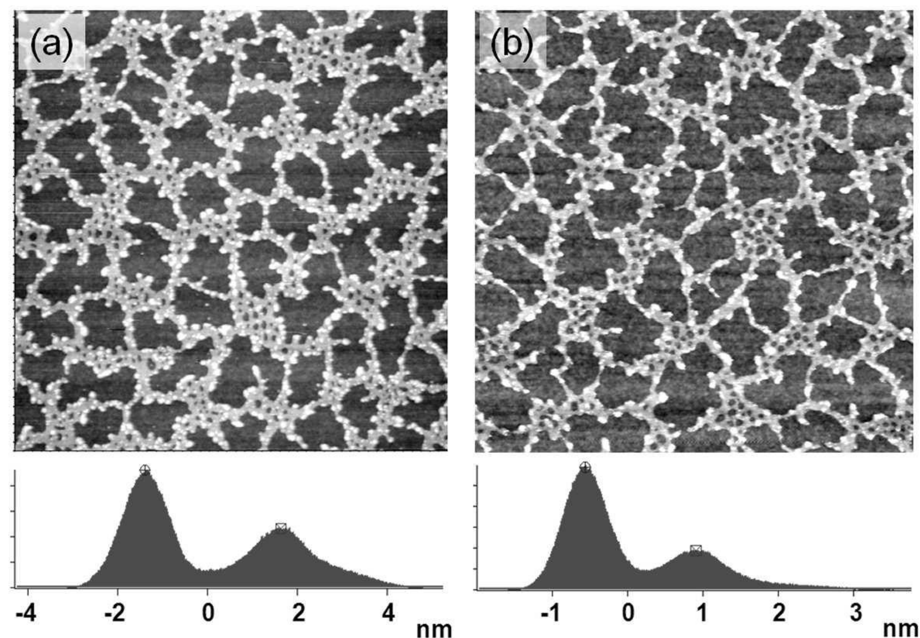

Figure 2. (a)A 2.5 x 2.5 μ m^2 image of a C_8-passivated Au nanoparticle network taken using attractive mode AFM imaging. For attractive mode imaging we chose the operating frequency, f, to be *greater than* the natural resonant frequency of the cantilever, f_0, ensure that the phase is $>$ 90 degrees, and lower the cantilever oscillation amplitude. In this case the imaging parameters were as follows: free cantilever oscillation amplitude: 0.3 V; amplitude setpoint: 0.23 V; driving frequency = +15% from free resonance at 79.407 kHz; Q gain =0.2. (b) A tapping mode image of the same network (although not the same region of the sample). Tapping mode parameters: free cantilever oscillation amplitude: 1 V; amplitude setpoint: 0.65 V; driven -5% from natural resonance at 79.174 kHz. The grey scale histograms show peaks arising from image contrast due to the nanoparticles and the underlying substrate. The separation of these peaks gives the mean height of the nanoparticles. In attractive mode (with the particular set of imaging parameters chosen in this case), the nanoparticle height is 3.0 nm, as compared to 1.5 nm in tapping mode imaging. The actual mean diameter of the (free) particles (core+thiols) is 4.3 nm. An AC240 cantilever was used for all measurements.

3.3 Frequency Shift vs Voltage Spectroscopy

Uncompensated electrostatic fields have been shown to play a key role in determining the apparent height of features in non-contact AFM images. In a careful and clever experiment, Yang et al.[29] used topographically flat Si(100) samples with regions of different doping type (n vs p) to show that work function differences of as little as 0.2 eV can produce height differences as large as a few nanometres (depending on the bias and properties of the tip). Similarly, a work function difference of only 50 meV was sufficient to lead to significant over-estimates (by as much as a factor of three) of the step height for C_{60} layers on graphite.[23] The passivated Au nanoparticle-SiO_2 system of interest here is particularly problematic comprising, as it does, not only four separate materials (Au nanoparticles, thiols, SiO_2, and the underlying silicon substrate) but involving two surface components (nanoparticles and SiO_2) which have radically different dielectric properties and conductivities. At room temperature, a C_8-passivated Au nanoparticle network is, if sufficiently interconnected, conducting, whereas the underlying silicon dioxide is, of course, insulating. Moreover, trapped charge at the silicon dioxide surface can affect not only the AFM imaging process but, as discussed in the context of the literature on the transport properties of nanostructured systems,[13,16,19] can strongly influence tunnelling-mediated charge pathways in nanoparticle arrays.

The electrostatic force, F_{EL} depends linearly on the gradient of the capacitance of the combined tip-sample system as a function of separation, $\frac{\partial C}{\partial z}$, and varies quadratically with the applied bias, V_B:

$$F_{EL} = -\frac{1}{2}\frac{\partial C}{\partial z}(V_B - V_{CP})^2 \quad (2)$$

where V_{CP} is the contact potential due to the difference in work function of the tip and sample. Setting V_B to match the contact potential should therefore null out the electrostatic orce due to the work function difference. In Fig. 3 we show Δf vs bias voltage plots for a Au nanoparticle network (in UHV) where the spectra have been

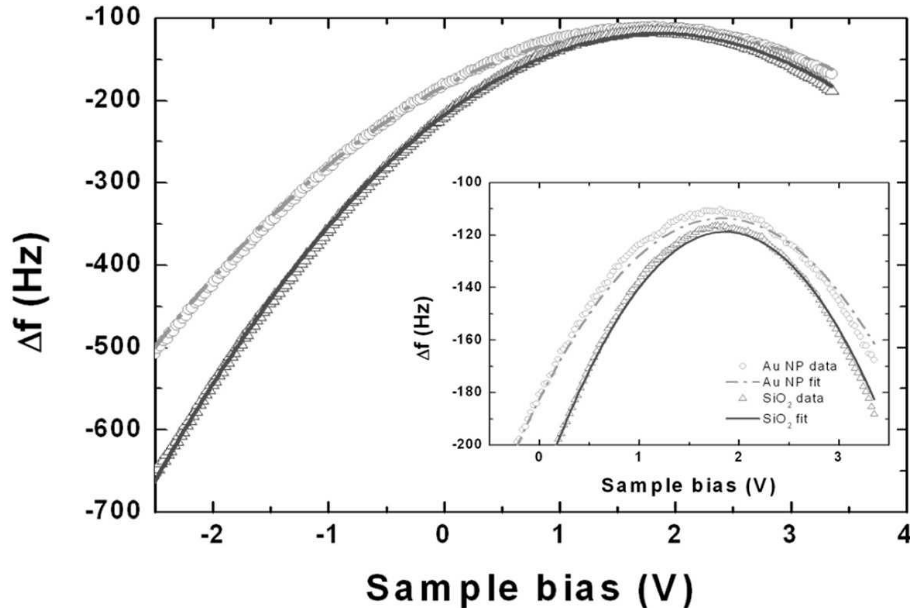

Figure 3. Frequency shift, Δf, vs bias voltage with the tip placed above the Au nanoparticle network (open circles) or the SiO_2 substrate (open triangles). The data are fit to a quadratic function, as described in the text, in each case. Inset: Magnification of graph close to the minimum frequency shift. A "super-sharp" silicon tip (NanoWorld) was used to acquire the data.

taken with the (silicon) tip above either a bare region of the SiO_2 substrate or above a Au nanoparticle-covered area (see also Fig. 4). In each case the experimental data (acquired with a "supersharp" silicon tip) are well fitted with the quadratic relationship given in Eqn. 2 above (although, as shown in the inset, the fit systematically deviates from the experimental data at the higher bias voltage end of the spectrum). Moreover, the noise in the data is thus that selecting V_B to an accuracy of better than 100 meV is not possible. It is also important to note that Jeffery *et al.*[30] found that the apparent contact potential difference (measured for a 7 nm thick silicon oxide layer with a metal-coated silicon probe) depended on the tip-sample separation and varied by a few hundred millivolts as the separation was changed by tens of nanometres.

Fig. 4 show images derived from a "spectromicroscopy" measurement, using the same "super-sharp" silicon tip, where at each point of a topographic image of the network, the feedback loop was broken and a frequency shift vs bias voltage curve was acquired. Following acquisition of the data, a particular bias voltage is selected and the variation in frequency shift across the surface for that voltage displayed, as in Fig. 4. The Au nanoparticle network is associated with a smaller frequency shift, and thus smaller electrostatic force, than the SiO_2 substrate throughout the bias voltage range (as can also be seen in Fig. 3). At positive bias voltages the difference in electrostatic force between the nanoparticle network and SiO_2 surface regions is much less pronounced until, at a voltage of 1.8 V - the minimum of the frequency shift vs bias voltage curve for both materials - the Au nanoparticle and SiO_2 regions can no longer be distinguished.

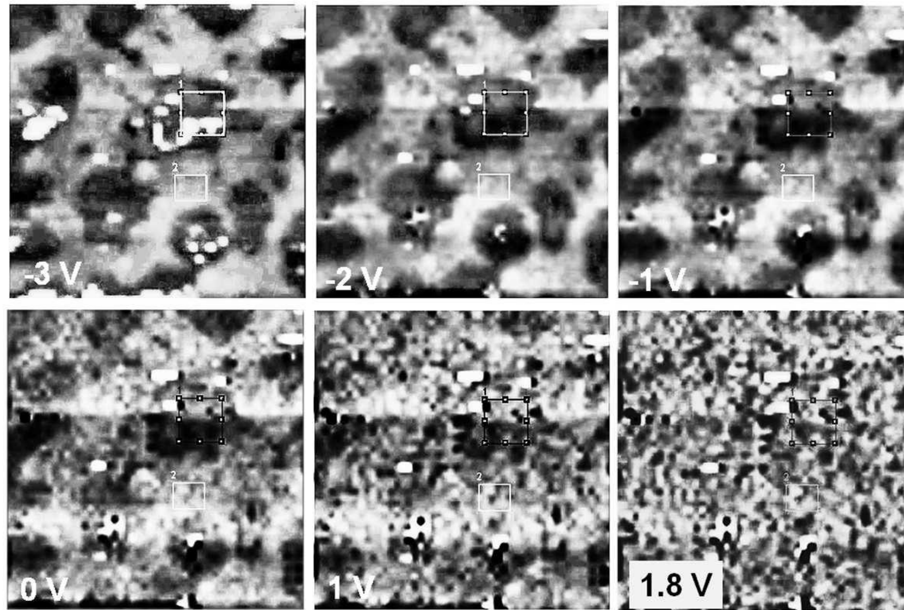

Figure 4. A set of images showing the variation in frequency shift across a Au nanoparticle network sample as a function of bias voltage (top row (l-r): -3V, -2 V, -1 V; bottom row (l-r): 0 V, +1 V, +1.8 V) , acquired using the "raster spectroscopy" mode of the UHV STM-AFM. Darker areas are associated with larger (more negative) frequency shifts. The data were acquired with a set-point cantilever vibration amplitude of 14.6 nm and, during the topographic imaging carried out in parallel with the spectroscopic imaging, a frequency shift of -115 Hz. A super-sharp silicon tip was used. The boxes in the images show the locations at which the spectra in Fig. 3 were acquired.

3.4 Force-Distance Spectroscopy: Measuring van der Waals and Electrostatic Forces

As noted in the preceding section, even small spatial variations in contact potential can lead to uncompensated electrostatic fields. In order to elucidate the contribution of these fields we have carried out Δf vs Δz spectroscopy. The Δf data are then converted to force data using the deconvolution process of Sader and Jarvis[26] (and a measurement of the cantilever oscillation amplitude). We carried out these measurements using a silicon

tip terminated with a tungsten needle (DP16-W, MikroMasch) in an attempt to improve spatial resolution in the measurements. (We note in passing that uncompensated electrostatic fields also have a very important influence on lateral resolution. See, for example, Sadewasser *et al.*[23]). Fig. 5 shows F vs z spectra taken on bare SiO_2 and Au nanoparticle regions of the surface with a DP16-W tip. In this case the mean contact potential was 3V (measured using Δf vs V spectroscopy) and the spectra and images shown in Fig.5 were thus taken with an applied bias of 3V. Although there is a very clear difference between the two force curves, both are associated with a long "tail" to higher separations, strongly suggesting that there is a residual electrostatic force. The inset to the figure shows a set of Δf images taken in the raster spectroscopy mode described in relation to Fig. 4. Note how the image contrast inverts as the tip moves away from the sample surface. This may arise from the increased dominance of electrostatic interactions over van der Waals forces at larger tip-sample separations.

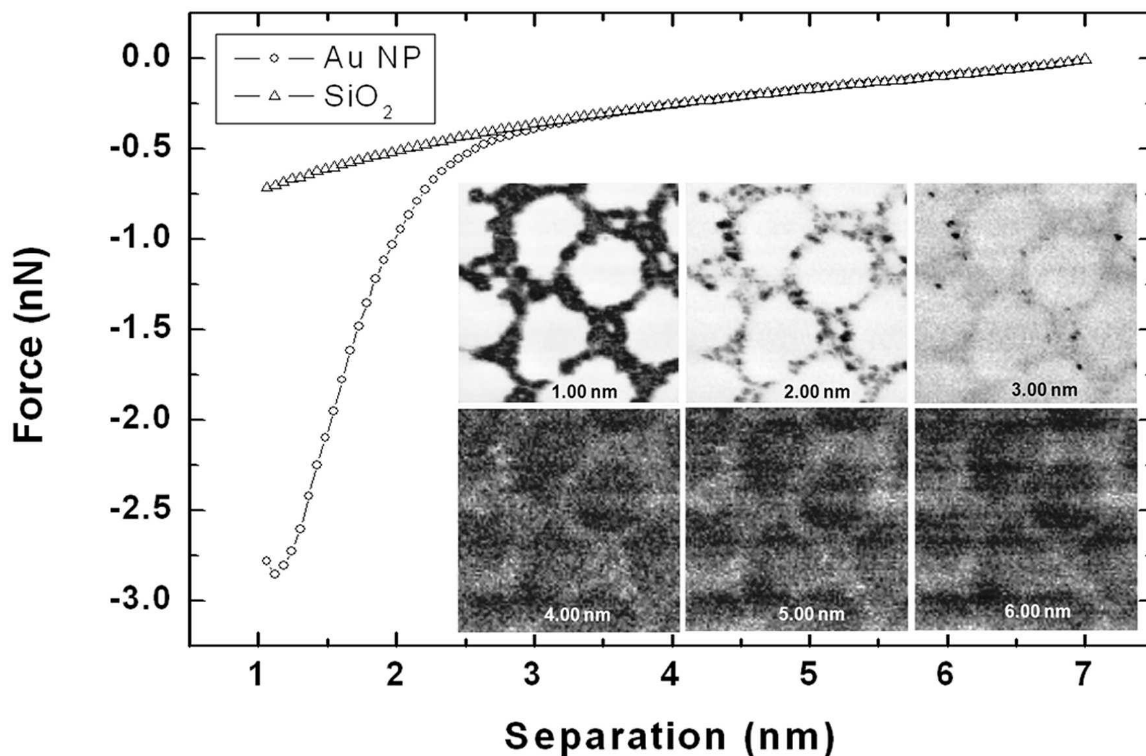

Figure 5. Force vs tip-sample separation data for a Au nanoparticle network on SiO_2 taken with a nominally tungsten-terminated DP16-W tip (see Experimental section for details of tip). Open triangles: area-averaged spectrum taken above bare SiO_2 surface region; open circles: area-averaged spectrum for Au nanoparticle (NP) region. Inset: maps of Δf taken in the ratser spectroscopy mode at various tip-sample separations. Note inversion of contrast. As for Fig. 4, darker regions in each map are associated with larger (more negative) frequency shifts.

In Fig. 6 we show the "long-range" components of the force curves with associated fits based on combining van der Waals and electrostatic interactions. Traditionally, van der Waals forces are fitted to the $\frac{1}{z^2}$ functional form arising from the interaction of a sphere with a plane, as described, for example, by Israelachvili.[31] The van der Waals force for a sphere interacting with a surface is:

$$F_{vdW} = -\frac{A_H R}{6z^2} \tag{3}$$

where A_H is the Hamaker constant associated with the dielectric properties of the sphere and the plane and R is the radius of the sphere. Electrostatic forces are typically (although certainly not always) modelled with a

function of the form R/z where R is the radius of curvature of the tip and z is the distance from the (conducting) plane. In our case, the sample surface contains both conducting (assuming percolating pathways through the nanoparticle network) and insulating regions. Hao *et al.*[32] considered a more realistic model of the tip and assumed an elongated cone profile. Using the image charge method they showed that the electrostatic force between the conical tip and the surface, F_{EL}, was given by:

$$F_{EL} \approx \frac{\lambda^2}{4\pi\epsilon_0} ln(\frac{L}{4z}) \tag{4}$$

where λ is the line density of the charge used in the conical model of the tip, and L is the effective cone length. Hao *et al.* also calculated the modification of the van der Waals force due to the consideration of a conical, rather than a spherical tip:

$$F_{vdW} = -\frac{A_H R}{6z^2} - A_H \frac{tan^2\theta}{6z} \tag{5}$$

where A_H is the unmodified Hamaker constant and θ is the cone half-angle. Importantly, for distances $z \ll R$, the correction to the standard result (Eqn.3) is negligible.

The solid line in Fig. 6 is a fit of the following function to the data:

$$F_{vdW} = -\frac{C_1}{z^2} - C_2 ln(\frac{C_3}{z}) \tag{6}$$

where $C_1 = A_H R/6, C_2$, and C_3 are constants. This combination of van der Waals and electrostatic terms provides a reasonable fit to the data, although the experimental measurements and fit clearly diverge at the extremes of the separation values. Although one could reasonably question the relevance of Eqn. 6 to the

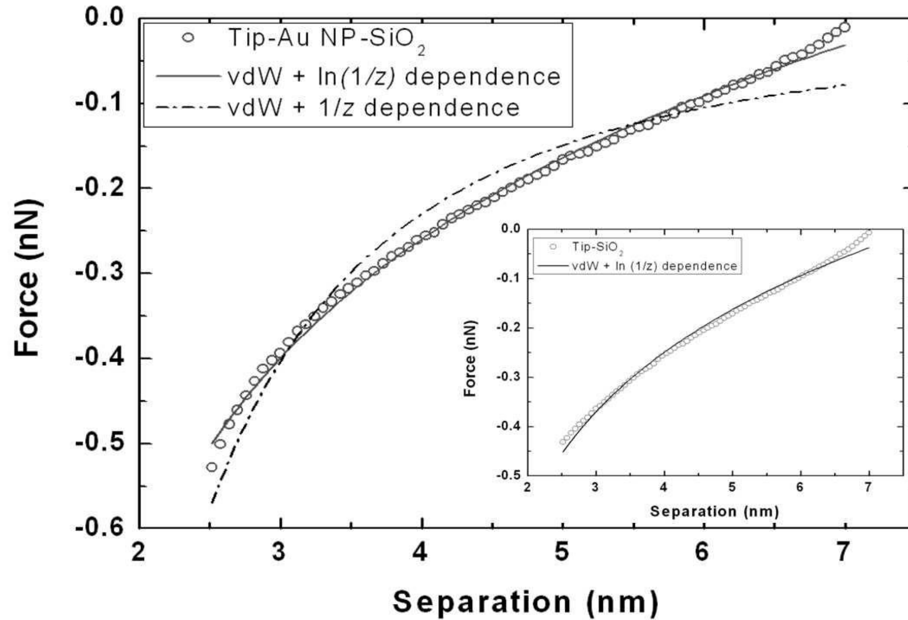

Figure 6. Open circles: force vs tip-sample separation (F vs z) spectrum for a DP16-W tip above a nanoparticle-covered region of the sample. The solid line is a fit using a combination of a van der Waals and an electrostatic term, as described in the text. Inset: Corresponding F vs z spectrum (and associated fit) measured above a region of bare SiO_2.

particular complex materials system studied here, attempts to fit the force curve with, for example, a $1/z$ dependence for the electrostatic force (see Fig. 6) or, indeed, with other power law dependencies produced much poorer fits (as was clear from the residuals spectrum (not shown) and the χ^2 value).

In principle, if we knew the true radius of curvature of the AFM tip we could extract a measurement of the Hamaker constant, A_H, for the combined tip-Au nanoparticle-SiO_2 system. If we use the nominal value of 1 nm for R, however, we extract unphysical values for the Hamaker constant (> 30 eV). If, instead, we take a value of 20 nm for R (which is more consistent with the observed imaging resolution of the tip and implies that the W tip has become blunted), the Hamaker constant for the W tip-Au NP-SiO_2 system is 1.5 eV. Sounilhac *et al.*[33] have measured a Hamaker constant of 0.8 ± 0.1 eV for the tungsten-SiO_2 system. Given that one might expect the Au-W interaction to increase the vdW force above that for a W-SiO_2 interaction, this estimate of A_H is reasonable. We stress again, however, that the estimate of A_H is based on an informed guess for the radius of curvature of the tip (and, indeed, assumes that the tip has not adsorbed nanoparticles while scanning). We are currently carrying out a series of experiments where scanning electron microscopy (complemented by X-ray analysis) and calibration standards comprising sharp asperities are used to characterise the tip shape before and after force measurements.

Finally, in the inset to Fig. 6 we show the force spectrum measured above a bare region of SiO_2. The solid line is a fit based on Eqn. 6 where C_1 has been fixed at a value consistent with the W-SiO_2 Hamaker constant determined by Sounilhac *et al.*[33] The fit is clearly much poorer than that for the data collected above Au nanoparticle regions, illustrating once again the difficulties associated with nulling electrostatic forces in this materials system.

4. CONCLUSIONS

Our atomic force microscopy measurements of self-organised Au nanoparticle assemblies on SiO_2/Si substrates highlight the difficulties associated with imaging complex multi-component systems with heterogeneous topographic and dielectric properties. The choice of imaging mode and scan parameters has a very strong effect on the measured height of the nanoparticles. In addition, the spatial variation of the dielectric properties makes accurate nulling out of electrostatic forces effectively impossible. It appears clear from our work to date that to accurately measure van der Waals forces, and their associated Hamaker constants, for this type of nanoparticle-dielectric system will necessitate the use of scanning Kelvin probe microscopy to minimise the electrostatic force at each point of the scan.

5. ACKNOWLEDGEMENTS

We are grateful for the financial support of the EU Framework Programme 6 Marie Curie scheme (under grant MRTN-CT-2004005728 (PATTERNS)). We also acknowledge funding from the UK Engineering and Physical Sciences Research Council (in the form of doctoral training account (DTA) PhD studentships). We thank the members of the PATTERNS network for helpful discussions regarding pattern formation in nanoparticle assemblies including, in particular, Uwe Thiele, Ulli Steiner, and Mathias Brust. It is also a pleasure to acknowledge very helpful discussions with James Sharp regarding both pattern formation and van der Waals forces/Hamaker constants. The small angle x-ray scattering work was performed on the EPSRC-funded XMaS beam line at the ESRF, directed by M.J. Cooper and C. Lucas. We are grateful to the beam line team of S.D. Brown, L. Bouchenoire, D. Mannix, D.F. Paul and P. Thompson for their invaluable assistance, and to Mark Everard, Chris Nicklin, and Richard Williams for both collaborating on the SAXS experiments and for helpful advice related to nanoparticle synthesis. Finally, we thank Juergen Koeble of Omicron Nanotechnology for his advice regarding the calibration of cantilever oscillation amplitudes.

REFERENCES

[1] Murray, C., Kagan, C., and Bawendi, M., "Synthesis and characterization of monodisperse nanocrystals and close-packed nanocrystal assemblies," *Ann. Rev. Mater. Sci.* **30**, 545 (2000).

[2] Pileni, M., "Self-assembly of inorganic nanocrystals: Fabrication and collective intrinsic properties," *Acc. Chem. Res.* **40**, 685 (2007).

[3] Martin, C., Blunt, M., Pauliac-Vaujour, E., Fahmi, A., DAleo, A., De Cola, L., Vögtle, F., and Moriarty, P., [*Self-organised Nanoparticle Assemblies: A Panoply of Patterns in "Systems Self-assembly: Interdisciplinary Snapshots"*].

[4] Ge, G. and Brus, L., "Evidence for spinodal phase separation in two-dimensional nanocrystal self-assembly," *J. Phys. Chem. B* **104**, 9573 (2000).

[5] Rabani, E., Reichman, D. R., Geissler, P. L., and Brus, L. E., "Drying-mediated self-assembly of nanoparticles," *Nature* **426**, 271 (2003).

[6] Moriarty, P., Taylor, M. D. R., and Brust, M., "Nanostructured cellular networks," *Phys. Rev. Lett.* **89**, 248303 (2002).

[7] Martin, C., Blunt, M., Pauliac-Vaujour, E., Stannard, A., Moriarty, P., Vancea, I., and Thiele, U., "Controlling pattern formation in nanoparticle assemblies via directed solvent dewetting," *Phys. Rev. Lett.* **99**, 116103 (2007).

[8] Maillard, M., Motte, L., and Pileni, M. P. *Adv. Mater.* **13**, 200 (2001).

[9] Martin, C., Blunt, M., and Moriarty, P., "Nanoparticle networks on silicon: Self-organized or disorganized?," *Nano Lett.* **4**(12), 2389 – 2392 (2004).

[10] Blunt, M., Martin, C., Ahola-Tuomi, M., Pauliac-Vaujour, E., Sharp, P., Nativo, P., Brust, M., and Moriarty, P., "Coerced mechanical coarsening of nanoparticle assemblies," *Nature Nanotech.* **2**(3), 167 – 170 (2007).

[11] Yosef, G. and Rabani, E., "Self-assembly of nanoparticles into rings: A lattice-gas model," *J. Phys. Chem. B* **110**, 20965 (2006).

[12] Pauliac-Vaujour, E., Stannard, A., Blunt, M., Martin, C., Notingher, I., Moriarty, P., Vancea, I., and Thiele, U., "Fingering instabilities in dewetting nanofluids," *Phys. Rev. Lett.* (2008).

[13] Parthasarathy, R., Lin, X., and Jaeger, H., "Electronic transport in metal nanocrystal arrays: The effect of structural disorder on scaling behavior," *Phys. Rev. Lett.* **87**(18) (2001).

[14] Parthasarathy, R., Lin, X., Elteto, K., Rosenbaum, T., and Jaeger, H., "Percolating through networks of random thresholds: Finite temperature electron tunneling in metal nanocrystal arrays," *Phys. Rev. Lett.* **92**(7) (2004).

[15] Rendell, R., Ancona, M., Kruppa, W., Foos, E., Snow, A., Park, D., and Boos, J., "Electron transport in nanocluster films with random voids," *IEEE Trans. Nanotech.* **2**(2), 75 – 81 (2003).

[16] Blunt, M., Suvakov, M., Pulizzi, F., Martin, C., Pauliac-Vaujour, E., Stannard, A., Rushforth, A., Tadic, B., and Moriarty, P., "Charge transport in cellular nanoparticle networks: Meandering through nanoscale mazes," *Nano Lett.* **7**(4), 855 – 860 (2007).

[17] Middleton, A. and Wingreen, N., "Collective transport in arrays of small metallic dots," *Phys. Rev. Lett.* **71**(19), 3198 – 3201 (1993).

[18] Elteto, K., Antonyan, E., Nguyen, T., and Jaeger, H., "Model for the onset of transport in systems with distributed thresholds for conduction," *Phys. Rev. B* **71**(6) (2005).

[19] Reichhardt, C. and Olson reichhardt, C. J., "Charge transport transitions and scaling in disordered arrays of metallic dots.," *Phys Rev Lett* **90**(4), 046802 (2003).

[20] Motte, L. and Pileni, M., "Self-assemblies of silver sulfide nanocrystals: influence of length of thio-alkyl chains used as coating agent," *Appl. Surf. Sci.* **164**, 60 – 67 (2000).

[21] Bain, C., Troughton, E., Tao, Y., Evall, J., Whitesides, G., and Nuzzo, R., "Formation of monolayer films by the spontaneous assembly of organic thiols from solution onto gold," *J. Am. Chem. Soc.* **111**, 321–335 (JAN 4 1989).

[22] Chen, L., Yu, X., and Wang, D., "Cantilever dynamics and quality factor control in ac mode afm height measurements," **107**(4-5), 275 – 280 (2007).

[23] Sadewasser, S., Carl, P., Glatzel, T., and Lux-Steiner, M., "Influence of uncompensated electrostatic force on height measurements in non-contact atomic force microscopy," **15**(2), S14 – S18 (2004).

[24] Stannard, A., Martin, C., Pauliac-Vaujour, E., Thiele, U., and Moriarty, P., "Dual-scale pattern formation in nanoparticle assemblies," (2008). submitted to J. Phys. Chem. C.

[25] Giessibl, F., "Advances in atomic force microscopy," *Rev. Mod. Phys.* **75**, 949 – 983 (2003).

[26] Sader, J. and Jarvis, S., "Accurate formulas for interaction force and energy in frequency modulation force spectroscopy," *Appl. Phys. Lett.* **84**(10), 1801 – 1803 (2004).

[27] Sader, J., Uchihashi, T., Higgins, M., Farrell, A., Nakayama, Y., and Jarvis, S., "Quantitative force measurements using frequency modulation atomic force microscopy - theoretical foundations," **16**(3), S94 – S101 (2005).

[28] Heyde, M., Kulawik, M., Rust, H.-P., and Freund, H.-J., "Frequency-modulated atomic force spectroscopy on nial(110) partially covered with a thin alumina film," *Phys. Rev. B* **73**(12) (2006).

[29] Yang, K., Chung, J., Hsieh, M., Ferng, S., Lin, D., and Chiang, T., "Systematic variations in apparent topographic height as measured by noncontact atomic force microscopy," *Phys. Rev. B* **74**(19) (2006).

[30] Jeffery, S., Oral, A., and Pethica, J., "Quantitative electrostatic force measurement in afm," *Appl. Surf. Sci.* **157**(4), 280 – 284 (2000).

[31] Israelachvili, J. N., [*Intermolecular and Surface Forces*], Academic Press, second ed. (1992).

[32] Hao, H., Baro, A., and Saenz, J., "Electrostatic and contact forces in force microscopy," *J. Vac. Sci. Tech. B* **9**(2), 1323 – 1328 (1991).

[33] Sounilhac, S., Barthel, E., and Creuzet, F., "The electrostatic contribution to the long-range interactions between tungsten and oxide surfaces under ultrahigh vacuum," *Appl. Surf. Sci.* **140**(3-4), 411 – 414 (1999).